Journal of Power Sources 191 (2009) 28–35

Contents lists available at ScienceDirect

Journal of Power Sources

journal homepage: www.elsevier.com/locate/jpowsour

Discharge mechanisms and electrochemical impedance spectroscopy measurements of single negative and positive lead-acid battery plates

C.V. D'Alkaine [a,*], P. Mengarda [b], P.R. Impinnisi [b]

[a] Group of Electrochemistry and Polymers, Chemistry Department, Federal University of São Carlos, 13560-905 São Carlos, SP, Brazil
[b] Battery Laboratory, Institute of Technology for Development - LACTEC, Curitiba, PR, Brazil

ARTICLE INFO

Article history:
Received 4 November 2008
Received in revised form 20 December 2008
Accepted 22 December 2008
Available online 30 December 2008

Keywords:
Lead-acid battery single plates
Charge/discharge mechanisms
Active material morphologies
EIS single plate data

ABSTRACT

This study interpreted open circuit impedance measurements of single negative and positive lead-acid battery plates, which were at different discharge levels and arranged in a four-electrode cell. This was performed in the framework of a proposed general model of charge/discharge reactions, morphological models of active materials, and based on interpretation of the characteristics of single negative and positive plates as measured by electrochemical impedance spectroscopy (EIS). This study shows that the proposed reaction models, morphological characteristics and EIS attributions are compatible with the obtained EIS data. The analysis indicates that negative and positive plate reaction mechanisms cannot be those proposed by the dissolution–precipitation mechanism alone. Rather, the reactions seem to obey the various mechanisms and morphologic ideas proposed in the present paper. It is shown that variations in the resistivity and dielectric constants of discharged films need to be studied in greater detail than film thicknesses to gain a better understanding of the processes.

1. Introduction

As discussed in a parallel paper in this issue [1], a critical review of the literature indicates that negative plates need to be thought of as having only macropores. This is because they yield practically the same area for Hg porosimeter and BET measurements [2]. In negative plates, the variation of BET area with respect to formation procedure [1] is much more restricted than that of positive plates [2]. Variation in BET area for negative plates can be explained as variation in the roughness of the macropore surface [1]. On the other hand, since positive plates present two very different levels of BET area (see in ref. [3]), it is necessary to introduce the existence of macropores and micropores to explain these two levels. These results reflect the fact that negative plate active material is a spongeous lead structure [4]. In contrast, positive plate active material is formed by particles that are bounded by necks, forming a coralline structure with micropores on the free surface of bounded particles [5]. As a consequence, charge/discharge reactions occur at the macropore surfaces of negative plates, and at macropore and micropore surfaces of positive plates.

The discharge reaction forms on negative electrodes through a solid-state mechanism, two types of $PbSO_4$ films [6]: (1) a glued $PbSO_4$ film, and (2) a disrupted $PbSO_4$ film that lies above the first. This does not mean that there is not a small amount of Pb^{2+} that dissolves at the beginning [7]. The glued film grows initially directly on the lead surface by a solid-state high electric field mechanism. The disrupted film is formed by partial rupture of the glued $PbSO_4$ film when the electric field through it decreases below a critical level, causing it to lose its stabilizing properties [6]. These phenomena have been found to occur in several metals and conditions [6]. The $PbSO_4$ glued film on Pb can easily be reduced to Pb by a high electric field mechanism, as voltammetric measurements have demonstrated [6]. The $PbSO_4$ disrupted films require the dissolution–precipitation mechanism for reduction to occur [6]. This last dissolution-diffusion process requires more time than that required by the high electric field process.

For positive flat electrodes, the existence of glued and disrupted films has also been demonstrated [8], although the author of the study did not state this conclusion. Without this conclusion, it would not be possible to explain how a considerable part of the voltammetric discharged PbO_2 can be recuperated in the following anodic sweep at $10\,mV\,s^{-1}$ [8]. This is an extremely high sweep velocity for a large portion of discharged PbO_2 to be re-oxidized by the dissolution–precipitation mechanism. The mechanism for film growth (reduction of PbO_2) or oxidation of the glued film is the high electric field mechanism, as for negative plates. Nevertheless, the glued film cannot be $PbSO_4$, because the SO_4^{2-} ion cannot enter the film against a reductive electric field [9]. It has been proposed that this film is

* Corresponding author. Tel.: +55 16 3351 8077; fax: +55 16 3351 8350.
E-mail address: dalkaine@dq.ufscar.br (C.V. D'Alkaine).

0378-7753/$ – see front matter © 2008 Elsevier B.V. All rights reserved.
doi:10.1016/j.jpowsour.2008.12.097

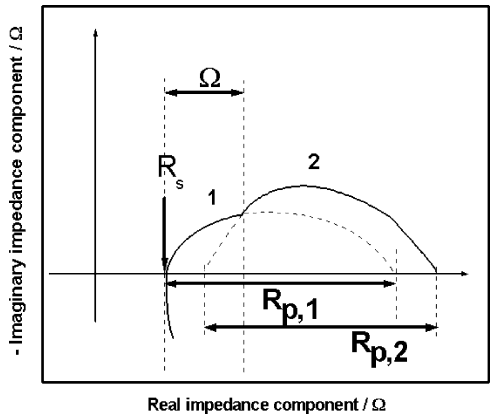

Fig. 1. Schematic imaginary impedance component/real impedance component plot of the three typical characteristic phenomena of EIS results for negative/positive lead-acid battery plates. (1) First capacity distributed loop; (2) second capacity distributed loop; $R_{p,1}$ polarization resistance of 1; $R_{p,2}$ polarization resistance of 2; R_s serial resistance and Ω, characteristic parameter.

some kind of PbO [10]. The existence of a disrupted $PbSO_4$ film, as well as the existence of a small amount of Pb^{2+} dissolution at the beginning of glued film formation, has never been questioned. In the positive plate, the disrupted $PbSO_4$ film is formed by disruption of the PbO glued film, followed by the reaction of disrupted PbO with H_2SO_4, because the electric field has disappeared.

Since glued and disrupted films exist at both negative and positive electrodes, charging processes always involve two steps. In the negative plate, the first step is recovery of the glued $PbSO_4$ film by its reduction through a solid-state high field mechanism [6]. This step is followed by reduction of the disrupted film via the direct dissolution–precipitation mechanism [11] or through the dissolution–precipitation mechanism in a narrow gap [8]. In the latter case, the active material reaction front (the narrow gap) advances in the direction of the disrupted film through a metasomatic process. For the positive plate, the two steps are equivalent to those in negative plates, although the glued film is a form of PbO instead of $PbSO_4$.

Electrochemical impedance spectroscopy (EIS) of negative and positive single plates shows three types of behaviors [12]. They present an inductive loop at high frequencies, a first capacity loop (1) at middle frequencies, and a second capacity loop (2) at low frequencies. These three behaviors can be seen schematically, together with different characteristic parameters, as plotted in Fig. 1. It is important to note the $R_{p,1}$ parameter can be considered as a polarization resistance related to the first (1) capacity loop, and the $R_{p,2}$ parameter is related to the second (2) capacity loop. These parameters will be determined and used in the present paper. The R_s parameter will also be used (Fig. 1). This is a serial resistance component at high frequencies, where impedance imaginary component of the inductive loop cancels with that of the first (1) capacity loop.

Many articles have been published on EIS measurements performed on single negative or positive lead-acid battery plates using a four-electrode configuration method [13]. Models and theories on electrochemical reaction processes were tested [14–17], physical and chemical plate characteristics were discussed [18–20], and the four-electrode method was shown to permit the determination of the working central plate impedance [21,22]. Nevertheless, relatively few publications interpret or examine the underlying cause of the detected EIS phenomena which have been summarized in Fig. 1. Thus, beginning with a detailed description of proposed morphologies and reaction mechanism models, including the attributions for different EIS phenomena, the present paper tests the proposed models and attributions for EIS data under different discharge conditions.

2. Experimental

Electrodes were lead-acid battery plates from stabilized VRLA stationary batteries of two different sizes and used in a two different cells of four electrodes setup. Central working electrodes measured 4.5 cm × 6.6 cm (geometrical double face area = 60 cm^2) and were taken from a 7 Ah, 12 V VRLA battery. For these electrodes, negative central plates had a C_{20} of 3.4 Ah, and positive central plates had a C_{20} of 3.9 Ah. Counter-electrodes were of two types obtained from the 7 Ah, 12 V VRLA battery or from a 600 Ah, 2 V VRLA battery. In this last case the plates' dimensions were 14.0 cm × 20.0 cm (total double face geometrical area = 560 cm^2) and both plates (positive and negative) had a C_{20} of 42 Ah and were overdimensioned to assure they will not suffer practical discharge during EIS measuring [22].

The experimental setup for discharge processes (discharge cell) was a four-electrode configuration, where the counter and working electrode geometrical areas were the same (4.5 cm × 6.6 cm). In the EIS measurement setup (the measuring cell), the working central electrodes were those from the 7 Ah, 12 V VRLA battery and always maintained at the center of the two side counter-electrodes. The side counter-electrodes were from the 600 Ah, 2 V VRLA battery, in a similar configuration as the discharge cell. Nevertheless, the area relation r, defined as the ratio of the counter-electrode geometrical area to the working electrode geometrical area, in the measuring cell, was 1.5. To obtain this area relation, the used counter-electrodes were partially immersed in the sulphuric acid solution, to a depth of 3.1 cm, yielding a 43.4 cm^2 area (3.1 cm × 14 cm).

To eliminate external electrolyte concentration changes, both cells were built with a 3-cm distance between working and counter-electrodes. This also reduced electrolyte concentration changes inside plate pores and permitted the introduction and removal of the central electrode.

The experimental procedure included: (1) discharging the central discharge cell electrode, (2) interrupting the discharge, (3) carrying the central electrode from the discharge cell to the EIS measuring cell, (4) waiting 2 h, (5) performing EIS measurements and (6) returning the central electrode to the discharge cell.

To assure that the depth of discharge (DOD) always corresponded to the same level of discharge, plates were full charged prior to any discharge, allowed to return to their reversible potentials and kept at this free electrode potential for some time.

EIS measuring cell counter-electrodes were maintained in a fully charged state in order to avoid any influence of their charge state on the EIS measurements. This was possible because they were used high capacity counter-electrodes.

In the EIS measuring cell, a 2-h rest time was always observed to eliminate possible concentration gradients inside central plate pores due to the discharge. EIS measurements were performed under a current perturbation of 10^{-3} A rms, in the linear region. The measuring frequency domain was from 10^4 to 10^{-2} Hz.

Electrode discharges were performed at a C_{18} discharge rate for negative plates, using a 3 mA cm^{-2} current density (double face) and at a C_{22} discharge rate for positive plates, using the same current density than in negative plates. Electrolyte solutions in both cells were always 4.6 M H_2SO_4. Reference electrodes in both cells were $Hg/Hg_2SO_4/4.6$ M H_2SO_4 and all the experiment were done at 25 °C.

The used equipment for charge/discharge and EIS measurements was a Gamry Potenciostat/Galvanostat/ZRA, serie G750, used always under galvanostatic conditions, together with the EIS300 Electrochemical Impedance Spectroscopy Software.

3. Results and discussion

Results will be analyzed first for negative plates and then for positive plates. Subsequently, these two ensembles of data will be compared. The analysis will be carried out using morphological and mechanistic models, including the attributions for different EIS phenomena, for negative and positive plates, proposed in the introduction and summarized in the next section. The main objective of the present work was to test the physical meanings attributed to different EIS characteristics.

3.1. Morphologies, models and EIS phenomena interpretations

Negative plates will be treated as if formed by a Pb spongeous structure containing only macropores with a certain surface roughness. Positive plates will be treated as though formed by a coralline structure containing macropores and micropores, with the origin of micropores at the surface of the macropores. On all inner surfaces of the active material, films were considered to grow in five stages: (1) small amount of initial Pb^{2+} dissolution, (2) nucleation and growth of the nuclei via solid-state reactions, (3) formation of a continuous film via collapse of nuclei, (4) growth of this film through a high electric field mechanism, and (5) partial disruption and recrystallization of the external portion of this film. For negative plates, both the glued and disrupted films were $PbSO_4$. For positive plates, the glued film was a type of Pb(II) solid film, possibly PbO, which when partially disrupted gives rise to a $PbSO_4$ disrupted film via reaction with H_2SO_4.

Based on these models different phenomena appearing in EIS measurements have received special physical attributions, which will be tested. The imaginary part at high frequencies (Fig. 1) has been attributed, fundamentally, to the inductive behavior of interconnected active materials in negative and positive plates. The first capacity loop (Fig. 1) in negative and positive plates has been attributed to reactions at the inner macropore surfaces. Finally, the second capacity loop (Fig. 1) in negative plates has been attributed to an inhomogeneous distribution of EIS perturbation current at the inner macropore surfaces. This inhomogeneous distribution is the result of inhomogeneities in film thickness. It seems that some types of CPE (Constant Phase Element) behavior [21] can arise from inhomogeneous current distribution. For positive plates, the second capacity loop has been attributed to reactions at the inner micropore surfaces. This is because researchers generally accept that in porous electrodes, when the frequency is reduced the alternating current perturbation advances in the direction of the inner porous material [22,23]. In positive plates, there are micropores at the surface of macropores, where the reaction can advance.

3.2. Negative plate results

In Fig. 2, a typical EIS result can be seen for a negative plate in its initial state, before the start of discharge.

EIS measurements of this initial state were always taken after a full charge followed by a waiting period, to permit the plate to come to its reversible potential. As a consequence of the auto-discharge during this waiting period, the negative active material should be assumed, from the point of view of the proposed model, to be covered on the macropore surfaces by a very thin glued $PbSO_4$ film, over which there is an extremely thin $PbSO_4$ disrupted film. Fig. 2 shows the normal inductive behavior at high frequencies. Based on the model described above, the inductive behavior is due to interconnected spongeous Pb together with connectors and external contributions. At middle frequencies a first capacity distributed loop appears, which is followed at lower frequencies by a constant phase element. The model predicts that the first capacity loop is due to the glued $PbSO_4$ film covered by a disrupted $PbSO_4$ film on the macropore surfaces. The estimated $R_{p,1}$ of the first capacity loop (see Fig. 1 for $R_{p,1}$ interpretation) was approximately 0.03 Ω (Fig. 3). The second capacity loop is attributed to the inhomogeneous EIS perturbation current distribution at the macropore surfaces. In this case it was not possible to calculate the $R_{p,2}$, which can be related to the CPE, for very low frequencies. This may be due to the frequency range used (up to only 10^{-2} Hz).

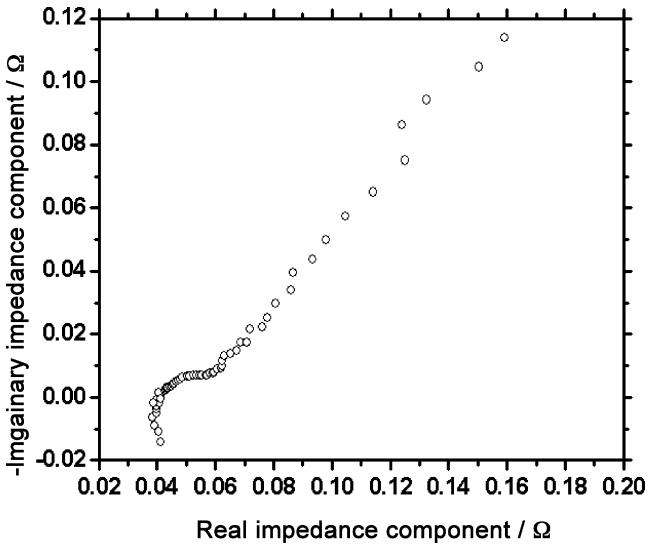

Fig. 2. Typical initial EIS data of a negative plate in its initial state, before the start of discharge. Plate area double face = 60 cm^2. Frequency range = 10^4–10^{-2} Hz.

It is interesting to note that, if the model is correct, not only would the first capacity distributed loop be present under different discharge conditions, but it would increase with increasing discharge. This would demonstrate the increase in glued film thickness during galvanostatic discharge. The glued film must grow on macropore surfaces, due to the increase of discharge. Disrupted films also must grow, since the disruption has had more time to occur. This phenomenon may not, however, affect EIS data, because it would present low resistance in comparison with the glued film resistance.

Typical EIS results at different partial discharge levels, DOD, are plotted for negative plates in Fig. 3. The DOD are given as a percentage of the total discharge, total DOD.

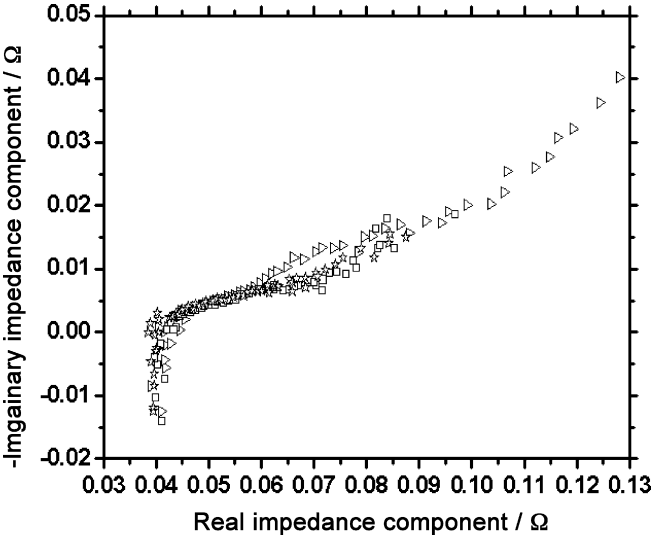

Fig. 3. Typical EIS data of a negative plate at different partial discharge levels (DOD). (☆) DOD = 30%; (□) DOD = 60%; (▷) DOD = 90%. Plate area double face = 60 cm^2. Frequency range = 10^4–10^{-2} Hz.

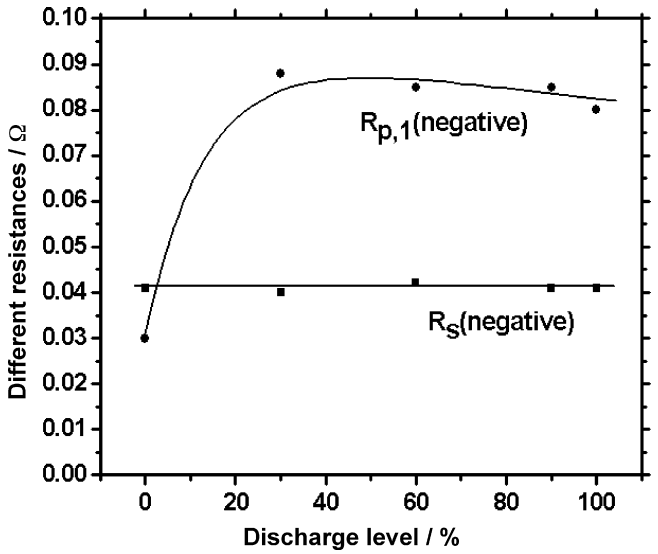

Fig. 4. Serie resistance (R_s) and polarization resistance of the first capacity loop ($R_{p,1}$) versus discharge level (DOD) for negative plates.

From Fig. 3, the R_S value (see Fig. 1 for R_S interpretation) is shown to change very little with DOD. This is consistent with the proposed model in that a spongeous structure should not be significantly perturbed in its electronic conductance (resistance), due to film formation on its surface.

Fig. 4 shows values of $R_{p,1}$ and R_S for different DOD, including the cases of total discharged and initial states. The constancy of R_S with DOD has been previously discussed. For $R_{p,1}$ of the negative plate, related to the first capacity loop, two effects must be considered. One is an increase in $R_{p,1}$ values up to approximately 40–50% of DOD, which the model attributes to the increase in thickness of the glued film. The second effect is a small decrease in $R_{p,1}$ after a DOD between 40% and 50%, which can be attributed to a reduction in average glued film thickness due to the disruption process. These considerations are based on the fact that the more important contribution to $R_{p,1}$ comes from the glued film thickness and considering that its ionic resistivity and the area are not important factors in this case.

Fig. 3 also points out that the real component of the second capacity loop starting point decreases at the end of the discharge. According to the model, this reflects increases in the inhomogeneities of EIS perturbation current distributions at inner macropore surfaces, which produce the second loop. This raises the question of why inhomogeneities appear at lower values for the real component of impedance at the end of the discharge. The reason may be that the increase in discharge increases the thickness of the glued film. This increase in thickness would be responsible for the appearance of film inhomogeneities, as a result of the increase of the disruption process. The film through which the EIS perturbation current flows at middle frequencies (first capacity loop) seems to look more homogeneous, because there are no differences in the EIS data for different DOD in this range of frequencies.

Fig. 3 also shows that there is a strong increase in the second capacity loop near the discharge end, in contrast to its nearly constant value during the initial and middle stages of discharge. This is consistent with the large increase in glued film thickness at the end of the discharge, once the entire macropore surface has been covered. The large increase in thickness is caused by the large increase in potential at the end of the discharge. On the other hand, the results of Fig. 3 as a whole are apparently inconsistent with the data from Fig. 2. This is because the real and imaginary components of the impedance are smaller in Fig. 3 than those in Fig. 2, for equivalent frequencies. An explanation for this apparent contradiction may be that the characteristics of the glued film change with DOD when going from the initial film to discharged ones. It is quite possible that the initial thin glued film has a higher resistivity and lower dielectric constants than films formed during discharge. Research on this point is ongoing.

In Fig. 5, a typical EIS result is shown for a totally discharged negative plate up to the cutting potential (−0.7 V). It is interesting for the model to note the strong increase in the second capacity loop magnitude at low frequencies compared to its magnitude in Fig. 3. This increase has begun to occur from a DOD of 90% in Fig. 3. The increase in second capacity loop contribution is interesting because, another time under the discharge conditions used (C_{18}), inhomogeneous distribution currents inside the plate inner surfaces become relevant only at the end of the discharge. In contrast, the capacity and resistance increases are consistent with the effects of the increase in the glued film thickness at the end of the discharge.

Finally, it is also interesting to note that, for a totally discharged negative plate (Fig. 5), the second distributed capacity loop shows quasi-diffusional behavior at the beginning of the loop, which becomes a CPE behavior at lower frequencies. An equivalent result has been reported in the literature (see Fig. 3 in ref. [23]).

3.3. Positive plate results

In Fig. 6, a typical EIS result is shown for the initial state of a positive plate, prior to the beginning of discharge. The three types of behavior found previously for the negative plate also appear in the figure: (1) an inductive behavior, at high frequencies; (2) a first capacity distributed loop, at middle frequencies; and (3) something resembling a complex capacity loop, at lower frequencies.

As for the negative plate, EIS measurements for the initial state of the positive plate were always made after a full charge followed by a waiting period, which allowed the plate to come to its reversible potential. Consequently, due to the auto-discharge during this waiting period, the positive active material at the initial state can be assumed, from the point of view of the proposed model, to be covered at macropore and micropore surfaces by an extremely thin glued PbO film. According to the model, also an extremely thin disrupted $PbSO_4$ film lies on top of the first one.

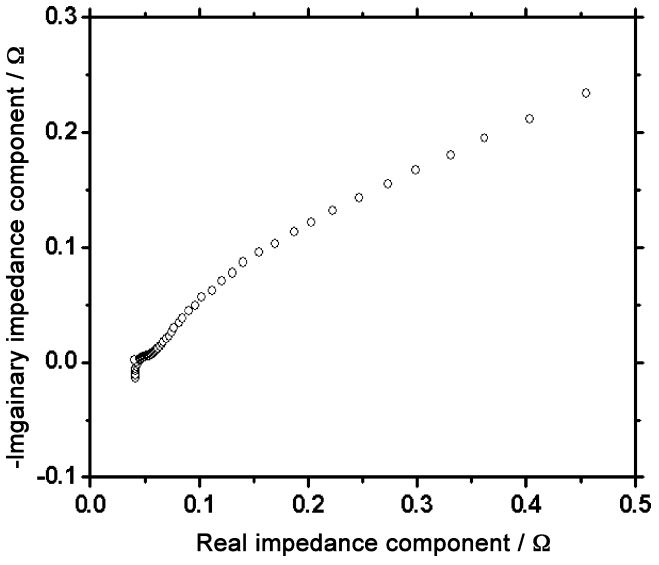

Fig. 5. Typical EIS data of a totally discharged negative plate up to the cutting potential (−0.7 V). Plate area double face = 60 cm^2. Frequency range = 10^4–10^{-2} Hz.

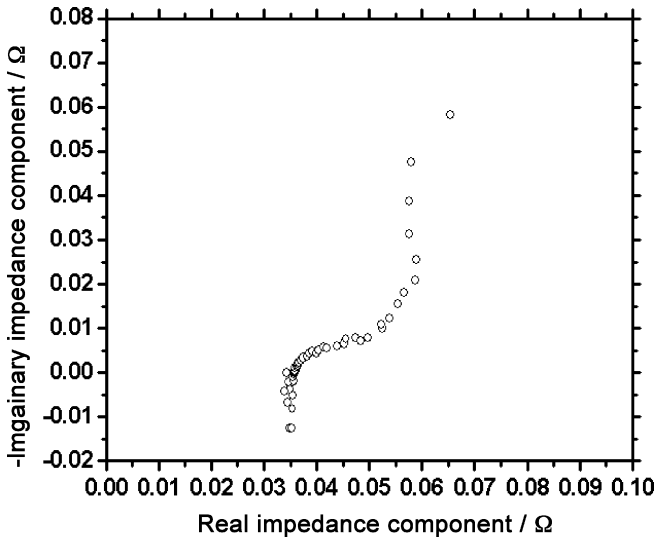

Fig. 6. Typical initial EIS data of a positive plate at the initial state before the beginning of the discharge. Plate area double face = 60 cm^2. Frequency range = 10^4–10^{-2} Hz.

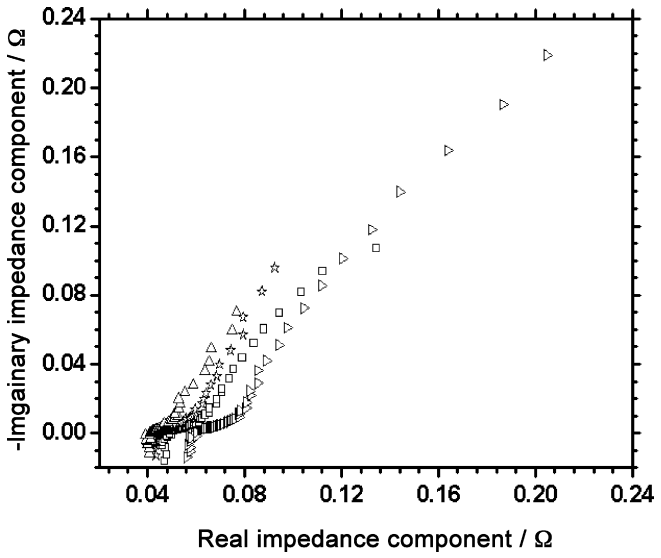

Fig. 7. Typical EIS data of a positive plate under different discharge levels (DOD). (△) DOD = 20%; (☆) DOD = 40%; (□) DOD = 60%; (▷) DOD = 80%. Plate area double face = 60 cm^2. Frequency range = 10^4–10^{-2} Hz.

In Fig. 6, inductive behavior at high frequencies is attributed to the interconnected, and now coralline structure of PbO_2, together with connectors and external contributions.

EIS a.c. perturbation penetrates more deeply into the PbO_2 porous structure as the frequency decreases. As a consequence, the results in Fig. 6 can be related to the different morphology of the negative and positive plates: the capacity loop at middle frequencies, with macropores; the complex capacity loop at low frequencies, with micropores. Since the discharge in this case occurs as a zone reaction going from macropores to micropores [10], the formation of a glued PbO film and subsequently the formation of disrupted $PbSO_4$ film follow the zone reaction sequence, going from macropores to micropores. Taking into account these facts for the positive plate model, the $R_{p,1}$ (see Fig. 1 for interpretation) would vary with film growth at the macropores, depending on the reaction zone area, if this last one advances through the macropores at the beginning of the discharge. For the initial state in Fig. 6, the $R_{p,1}$ value was found to be 0.04 Ω. In contrast, as for the negative case, it was not possible to calculate the $R_{p,2}$ (see Fig. 1 for interpretation).

Positive plate measurements at different discharge levels (Fig. 7) showed that the first capacity loop seemed to remain constant, while the second capacity loop grew fundamentally at the end of the discharge. These facts can be interpreted based on the proposed positive plate model, considering that the film seems to be present over the entire macropore surface from the beginning of discharge ($R_{p,1}$ is constant in Fig. 8), but it advanced into the micropore during the increase in DOD (the second capacity loop slightly increases during discharge, see Fig. 7). The fact that $R_{p,1}$ remains constant for different levels of discharge implies, taking into account the proposed model, that the product of film thickness and resistivity seems to remain essentially constant.

Finally, it appears that at the end of discharge, a substantial decrease in free micropore area available for film growth occurs. This decrease gives rise to an even greater increase in the glued film thickness at micropores because there is an increase of the second capacity loop at the end of the discharge (see Fig. 7).

As a consequence of all the above discussions, the positive plate is predicted to have two variable impedances in parallel, during the discharge. One is referred to the areas where glued films are growing (Z_{gf}) and the other is referred to the areas containing the initial thin film that has yet to grow (Z_{thf}); the latter seems to occur mostly at micropore surfaces. These two parallel impedances can give different total impedance Z behaviors (increasing or decreasing $|Z|$ with the discharge) when the EIS data of different discharge levels are compared. This is because it will vary the related areas of Z_{thf} and Z_{gf} together with the thickness and the dielectric constants corresponding to Z_{gf} (l_{gf} and ε_{gf}, respectively), while the thickness and dielectric constants corresponding to Z_{thf} (l_{thf} and ε_{thf}, respectively) will remain practically constant. For the initial state of discharge there will be only Z_{thf} (Fig. 6) and for the final state of discharge, up to the cutting potential (Fig. 9), only Z_{gf} with its corresponding l_{gf} and ε_{gf}.

In Fig. 8, the increase of R_s may be explained by the idea that an increase in discharge level compromises the necks between particles in the coralline structure of positive plates, which provides evidence that such coralline structure exists.

Fig. 9 shows a typical EIS for a positive plate that is totally discharged up to the cutting potential (1.05 V). In this case the Z_{thf} is not more present since the electrode is now completely covered by the two films at the end of the discharge (glued PbO and dis-

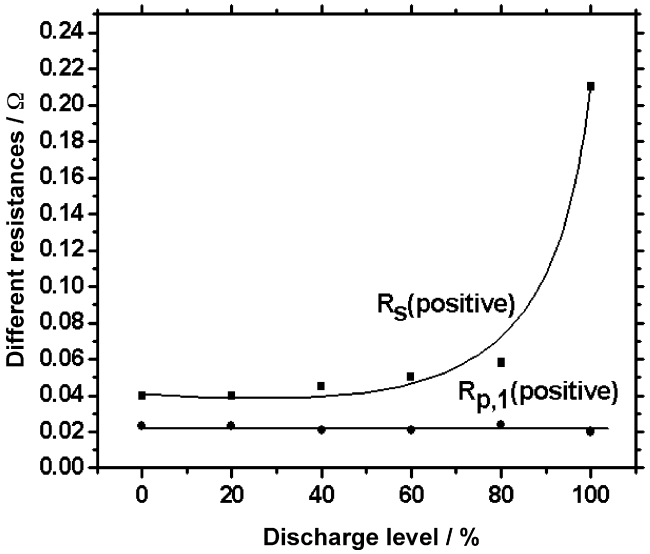

Fig. 8. Serie resistance (R_s) and polarization resistance of the first capacity loop ($R_{p,1}$) versus discharge level (DOD) for positive plates.

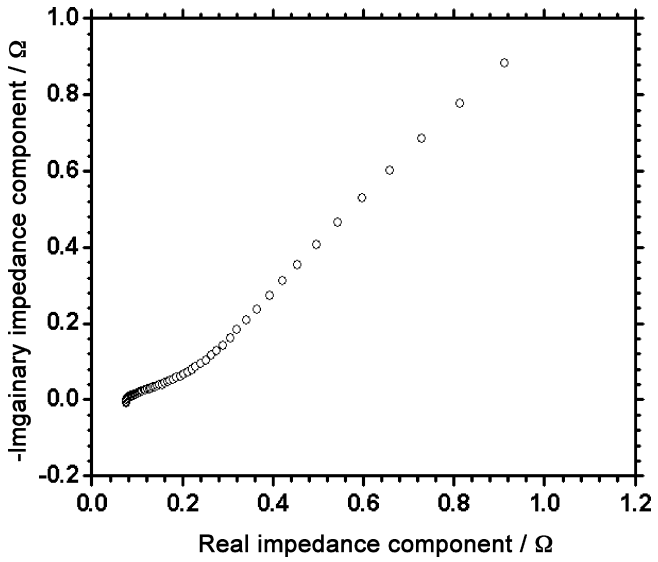

Fig. 9. Typical EIS data of a totally discharged positive plate up to the cutting potential (1.05 V). Plate area double face = 60 cm^2. Frequency range = 10^4–10^{-2} Hz.

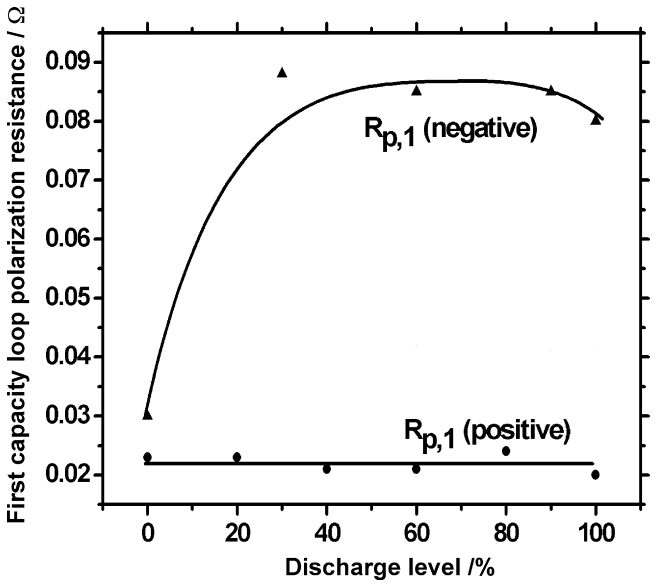

Fig. 11. Polarization resistance of the first capacity loop ($R_{p,1}$) versus discharge level (DOD) for negative (▲) and positive (●) plates.

rupted $PbSO_4$) at macropores and micropores. The model predicts that under these conditions, the system has only one component (Z_{gf}). The second capacity loop is even greater than at lower discharge levels (compare Fig. 9 with Fig. 7, especially DOD 80% in the latter). This is consistent with an increase in the thickness of glued film, which increases film resistance and decreases its capacity inside micropore areas. The R_S value (Fig. 9) increases even more than before (Fig. 8) due to discharge films at the necks and $R_{p,1}$ retains the same value of the other discharge levels.

3.4. Comparison between negative and positive plate results

Several interesting aspects must be pointed out when comparing negative and positive single plate EIS data.

The comparison between EIS measurements of the negative and positive initial states (Fig. 10) shows that the imaginary and real components of the observed impedances are higher for the negative plates than for the positive ones for the same frequency; this is consistent with the fact that negative plates have a BET area approximately 10 times smaller than positive ones [2]. These results are consistent with the proposed model, which predicts that the imaginary and real components are proportional to the inverse of the BET area. Differences in the resistivity and dielectric constants between the two glued films, $PbSO_4$ and PbO, seem not to be the main factors to determine the order of magnitude of the impedance module differences at the initial states.

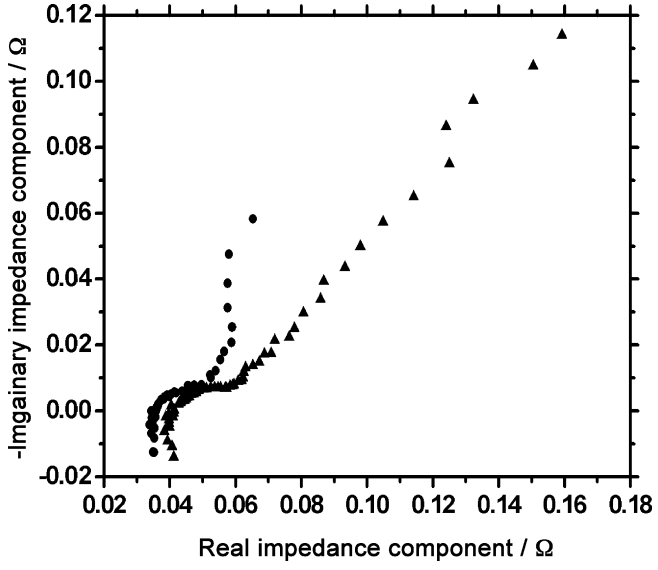

Fig. 10. Comparison between typical initial EIS data of negative (▲) and positive (●) plates at the initial state before the beginning of the discharge (0% DOD).

Another interesting point about the EIS of negative and positive initial states is that the second capacity loops at low frequencies are different (Fig. 10). This is consistent with the models, which holds that the second capacity loop in negative plates is related to an inhomogeneous EIS perturbation current distribution at macropore surfaces and in positive plates, in contrast, it is related to the existence of micropores.

When comparing different negative and positive plate discharge levels (Fig. 11), it is worth noting that $R_{p,1}$ increases for negative plates and then slowly decreases with farther discharge level increase. For positive plates, in contrast, $R_{p,1}$ remains essentially constant for any DOD (Fig. 11), indicating that the discharge processes must be different for the two plates. This fact is inconsistent with the dissolution–precipitation mechanism because this proposition presupposes the same mechanisms, but it is consistent with the reaction models presented here. The Fig. 11 shows that $R_{p,1}$ (negative) is greater than $R_{p,1}$ (positive) except at the initial states. The $R_{p,1}$ results for the first distributed capacity loop correspond, following the proposed models, to reactions occurring in macropore areas as seen for the Hg porosimeter. The average area measured for positive plates using the Hg porosimeter method is slightly higher than for negative plates [2], in agreement with the previous result. This proves the importance of the differences found in areas measured at negative and positive plates by the Hg porosimeter technique. If this is so, the ratio of $R_{p,1}$(negative)/$R_{p,1}$(positive) for totally discharged plates should give an idea of the relationship between the values for the inverse of the Hg porosimeter macropore area in the negative and positive cases. This ratio gives approximately 4, which agrees with the value calculated using Hg porosimeter results (calculated from ref. [2]). This reasoning does not take into account the variations in resistivity.

The constancy in R_S for negative plates and its increase for positive plates during discharge (Fig. 12) supports the idea that negative

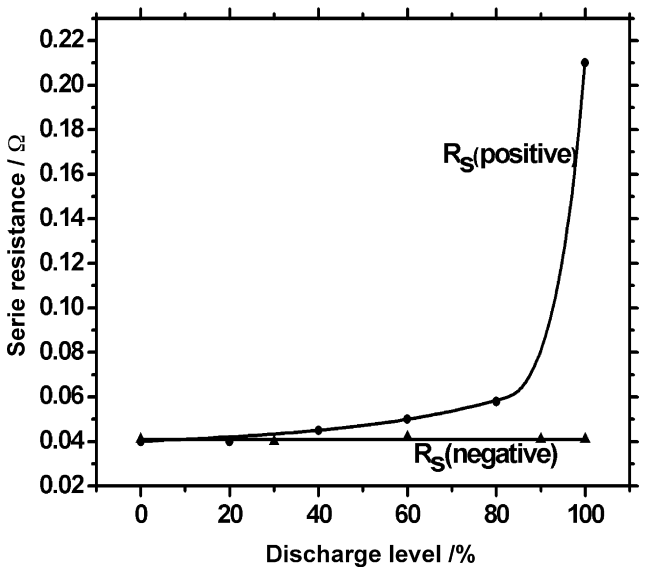

Fig. 12. Serie resistance (R_s) versus discharge level (DOD) for negative (▲) and positive (●) plates.

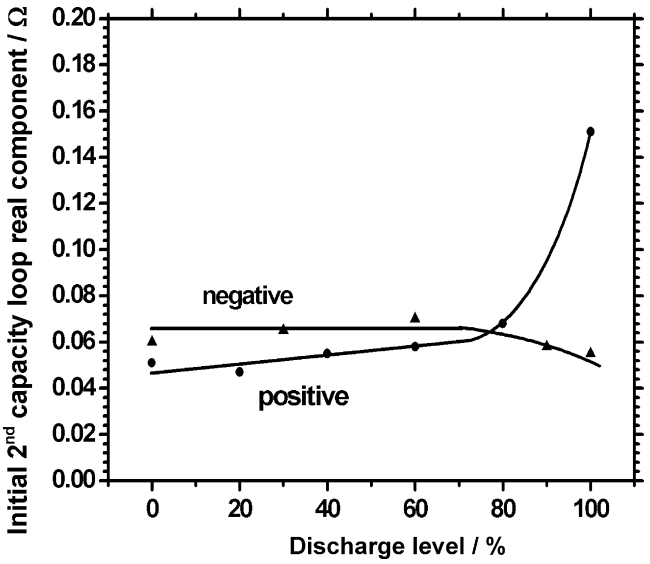

Fig. 14. Initial capacity loop real component versus discharge level (DOD) for negative (▲) and positive (●) plates.

plates are made up of a spongeous Pb matrix, while positive plates are made up of PbO_2 particles connected by necks, giving rise to a three-dimensional coralline framework. Fig. 12 shows that the R_s for negative plates is lower than for positive plates, principally after different discharge levels. This is presumably due to the existence of a spongeous Pb structure for negative plates and a coralline structure for positive plates where the necks are compromised during discharge.

On the other hand, EIS data for negative and positive plates in Fig. 13 seem to contradict each other, if only the greater BET active area for positive plates over negative plates is taken into account. In Fig. 13, real and imaginary components of negative plates are lower than positive ones. This can be explained by the model proposed here, considering that the product of resistivity multiplied by thickness or that of the dielectric constant divided by thickness will be different for the two glued films ($PbSO_4$ for negative plates, and PbO for positive plates). The difference cannot be explained only by different film thickness. However, it can be explained by the variation in film properties between negative and positive plates.

In Fig. 14, it is seen that the shifts of the starts of the second capacity distributed loops on the real axis of negative and positive plates (obtained from Figs 2, 3 and 5 for negative and Figs. 6, 7 and 9 for positive plates) present different behaviors and then must obey to different causes. In the negative plate a shift only occurs at the end of the discharge and to lower values of the real axis, in agreement with the increase of the inhomogeneity of the glued $PbSO_4$ film at the end of the discharge. In the positive plate the shift is to higher values of the real axis and for any discharge level, mainly at the end of the discharge. From Fig. 7, the shift in the positive case is clearly due to the shift of the first capacity loop. Actually, this is not a real shifting of the first or the second capacity loops, it is only the consequence of the increase of the value of R_s with the discharge (see Fig. 7). This is why it occurs from the beginning of the discharge, like the increase of R_s. These analyses again indicate the need to invoke different mechanisms for the second capacity

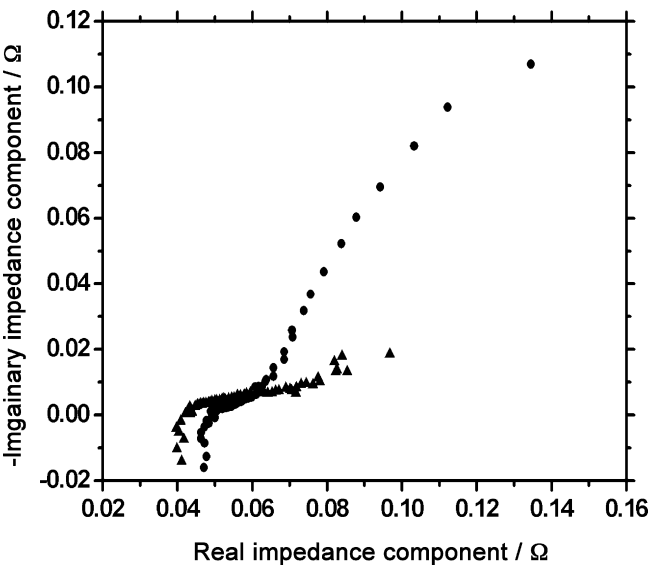

Fig. 13. Comparison between typical EIS data of negative (▲) and positive (●) plates under 60% discharge level (60% DOD).

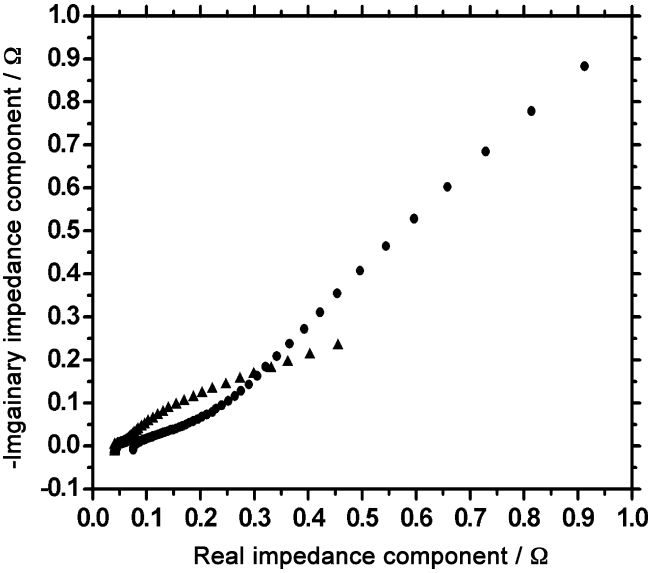

Fig. 15. Comparison between typical EIS data of a totally discharged negative (▲) and positive (●) plates up to the respective cutting potentials (100% DOD).

loop at the negative and positive plates, as the proposed models do.

Finally, it is necessary to compare the EIS results for totally discharged plates up to the cutting potentials (Fig. 15). The interesting point is that in the low frequency region, negative plates show a lower second capacity loop than that of positive plates, which is inconsistent with the fact that the former have a BET area approximately 10 times smaller than positive plates. This shows that, at low frequencies, in negative and positive plates the EIS data see different phenomena as proposed.

4. Conclusions

To explain positive and negative single plate EIS results, the literature on plate morphology and reaction mechanism models is critical reviewed and models are presented on this base. In these models, negative plates are considered to be made up of a lead spongeous structure with only macropores, with films of different thicknesses during discharge. Positive plates are considered to be made up of a coralline structure with macropores and micropores, with the latter having their origin on the surface of the former. The models propose that a thin glued film grows on the inner surfaces of negative and positive plates, and a disrupted film forms over the thin glued film. For negative plates, both the glued and disrupted films are $PbSO_4$. For positive plates, the glued film is a type of PbO. This film, after its partially disruption gives rise to a $PbSO_4$ disrupted film by reaction with H_2SO_4.

These models are used to interpret the three different phenomena recorded in EIS lead-acid battery plate measurements. The inductive loop at high frequencies is mainly attributed in negative and positive plates to the inductive behavior of interconnected active materials. The first capacity loops in negative and positive single plates at middle frequencies are attributed to film growth at inner macropore surfaces. Finally, for negative plates, the second capacity loop at low frequencies is attributed to inhomogeneous film growth at inner macropore surfaces, which gives rise to an inhomogeneous distribution of EIS perturbation currents. These inhomogeneities appear because the increase in discharge also increases the glued film thickness, which in turn increases the disruption process and generates film inhomogeneities. For positive plates, the second capacity loop is attributed to glued film growth at inner micropore surfaces.

In order to explain the empirical EIS data it was necessary, in some cases, to take into account the glued film resistivity and dielectric constants, together with variations in film thickness.

The whole analysis shows that discharge processes at negative and positive single plates cannot be explained using only the dissolution–precipitation model. Two different models are proposed here that do account for the different processes at both positive and negative plates.

Acknowledgment

The authors are grateful to the Paraná Energy Company-Copel for financial support.

References

[1] C.V. DïAlkaine, G.A.O. Brito, J. Power Sources, doi:10.1016/j.jpowsour.2009.02.002, submitted for publication.
[2] E.E. Ferg, P. Loyson, N. Rust, J. Power Sources 141 (2005) 316–325.
[3] L.T. Lam, O. Lim, H. Ozgun, D.A.J. Rand, J. Power Sources 48 (1994) 83–111.
[4] D.S. Rand, D.P. Boden, C.S. Lakshmi, R.P. Nelson, R.D. Prengamann, J. Power Sources 107 (2002) 280–300.
[5] D. Pavlov, G. Petkova, M. Dimitrov, M. Schiomi, M. Tsubota, J. Power Sources 87 (2000) 39–56.
[6] C.V. D'Alkaine, C.M. Garcia, P.M.M. Pratta, G.A.O. Brito, F.P. Fernandes, J. Solid State Electrochem. 11 (2007) 1575–1583.
[7] F.E. Varela, M.E. Vela, J.R. Vilche, A.J. Arvia, Electrochim. Acta 38 (11) (1993) 1513–1520.
[8] Z. Takehara, J. Power Sources 85 (2000) 29–37.
[9] C.V. DïAlkaine, Conference UNESCO Expert Workshop: Theory and Practice of Lead Acid Systems, Dresden, Gaussig Castle, Germany, 1991.
[10] C.V. D'Alkaine, A. Carubelli, M.C. Lopes, J. Power Sources 64 (1997) 111–115.
[11] C.V. D'Alkaine, L.M.M. de Souza, P.R. Impinnisi, J. de Andrade, J. Power Sources 158 (2006) 997–1003.
[12] M. Keddam, C. Rakatomavo, H. Takenouti, in: R.K. Bullock, D. Pavlov (Eds.), Advanced in Lead Acid Batteries, The Electrochemical Soc. Inc., 1984, pp. 277–280.
[13] F. Huet, J. Power Sources 70 (1998) 59–69.
[14] A. Kirchev, A. Delaille, M. Perrin, E. Lemaire, F. Mattera, J. Power Sources 170 (2007) 495–512.
[15] A. Terno, R. Terno, T. Suntio, J. Electrochem. Soc. 151 (6) (2004) A806–A824.
[16] M. Thele, E. Karden, E. Surewaard, D.U. Sauer, J. Power Sources 158 (2006) 953–963.
[17] M. Hejabi, A. Oweisi, N. Gharib, J. Power Sources 158 (2006) 944–948.
[18] J. Jindra, M. Musilová, J. Mrha, A.A. Taganova, J. Power Sources 37 (1992) 403–409.
[19] F. Huet, R.P. Nogueira, P. Lailler, L. Torcheux, J. Power Sources 158 (2006) 1012–1018.
[20] D. Pavlov, G. Petkova, J. Electrochem. Soc. 149 (5) (2002) A654–A661.
[21] A.L. Van Den Eeden, Metal Structure and Double Layer Capacity. Quantum-chemical Model Calculations on Clusters, Thesis, Utrecht University, 1955, pp. 78–79.
[22] C.V. DïAlkaine, G.A.O. Brito, C.M. Garcia, P.R. Impinnisi, Impedance Contributions Online 6 (2008) P2-1–P2-18, http://accessimpedance.iusi.bas.bg, Web Journal, European Internet Centre for Impedance Spectroscopy (EICIS).
[23] D.D. Macdonald, Electrochimica Acta 51 (2006) 1376–1388.